

Discreditation of bobdownsite and the establishment of criteria for the identification of minerals
with essential monofluorophosphate (PO_3F^{2-})

Francis M. McCubbin^{1,2}, Brian L. Phillips³, Christopher T. Adcock⁴, Kimberly T. Tait⁵, Andrew
Steele⁶, John S. Vaughn³, Marc D. Fries¹, Viorel Atudorei⁷, Kathleen E. Vander Kaaden⁸,
Elisabeth M. Hausrath⁴

¹ NASA Johnson Space Center, Mailcode XI2, 2101 NASA Parkway, Houston, TX 77058, USA

² Institute of Meteoritics, MSC03 2050, University of New Mexico, 200 Yale Blvd SE,
Albuquerque, NM 87131, USA

³ Department of Geosciences, Stony Brook University, Stony Brook, NY 11794-2100, USA

⁴ Department of Geoscience, University of Nevada, Las Vegas, Las Vegas, NV, 89154, USA

⁵ Department of Natural History, Royal Ontario Museum, 100 Queen's Park, Toronto, Ontario
M5S 2C6, Canada

⁶ Geophysical Laboratory, Carnegie Institution of Washington, 5251 Broad Branch Rd., N.W.,
Washington, DC 20015, USA

⁷ Department of Earth and Planetary Sciences, University of New Mexico, 200 Yale Blvd SE,
Albuquerque, NM 87131, USA

⁸ Jacobs Technology, NASA Johnson Space Center, Mailcode XI, 2101 NASA Parkway,
Houston, TX 77058, USA

Abstract

Bobdownsite, IMA number 2008-037, was approved as a new mineral by the Commission on New Minerals, Nomenclature and Classification (CNMNC) as the fluorine endmember of the mineral whitlockite. The type locality of bobdownsite is in Big Fish River, Yukon Canada, and bobdownsite was reported to be the first naturally occurring mineral with essential monofluorophosphate (PO_3F^{2-}). The type specimen of bobdownsite has been reinvestigated by electron probe microanalysis (EPMA), and our data indicate that fluorine abundances are below detection in the mineral. In addition, we conducted detailed analysis of bobdownsite from the type locality by gas chromatography isotope ratio mass spectrometry, Raman spectroscopy, EPMA, and NMR spectroscopy. These data were compared with previously published data on synthetic monofluorophosphate salts. Collectively, these data indicate that bobdownsite is indistinguishable from whitlockite with a composition along the whitlockite-merrillite solid solution. Bobdownsite is therefore discredited as a valid mineral species. An additional mineral, krásnoite, has been purported to have monofluorophosphate components in its structure, but reexamination of those data indicate that F^- in krásnoite forms bonds with Al, similar to OH^- bonded to Al in perhamite. Consequently, krásnoite also lacks monofluorophosphate groups, and there are currently no valid mineral species with monofluorophosphate in their structure. We recommend that any future reports of new minerals that contain essential monofluorophosphate anions be vetted by abundance measurements of fluorine, vibrational spectroscopy (both Raman and FTIR), and where paramagnetic components are permissibly low, NMR spectroscopy. Furthermore, we emphasize the importance of using synthetic compounds containing monofluorophosphate anions as a point of comparison in the identification of minerals with essential monofluorophosphate. Structural data that yield satisfactory P-F bond lengths determined by X-ray crystallography, coupled with direct chemical analyses of fluorine in a material do not constitute sufficient evidence alone to identify a new mineral with essential monofluorophosphate anions.

Introduction

Phosphate minerals such as apatite, merrillite, and whitlockite are of importance to a wide variety of fields, from Earth science to life science, material science, and planetary science (Chew and Spikings, 2015; Harlov, 2015; Hawthorne, 1998; Hughes et al., 2006; Hughes et al., 2008; Hughes and Rakovan, 2015; Jolliff et al., 2006; McCubbin and Jones, 2015; McCubbin et al., 2014; Rakovan and Pasteris, 2015; Shearer et al., 2015; Webster and Piccoli, 2015). Phosphates are the major source of P on Earth and their uses range from fertilizers to detergents to insecticides. Synthetic phosphates have been used for ceramics and coatings, and have even been used for the production of fuel cells (i.e., Kendrick et al., 2007; Lin et al., 2007; Pietak et al., 2007). Phosphates have a propensity for concentrating rare earth elements (Jolliff et al., 1993; Prowatke and Klemme, 2006; Shearer et al., 2011), which are used pervasively for deciphering sedimentary, igneous, and metamorphic petrogenesis. Furthermore, their ability to accommodate the radioisotopes used for dating makes them important to geochronological studies of rocks (Chew and Spikings, 2015).

At present, there are 586 unique phosphate mineral species that have been identified (Hazen et al., 2015; IMA list of minerals updated as of January 2017). Of these, the phosphate anion is most typically represented by phosphate (PO_4^{3-}), where phosphorus is bonded to 4 oxygens; however, there is a subset of phosphate minerals totaling 58 individual mineral species that have OH^- or F^- substituents for O^{2-} on the phosphate molecule. These substituents consist of either hydrogen phosphate anions ($\text{PO}_3\text{OH}^{2-}$) or monofluorophosphate anions (PO_3F^{2-}). Minerals with protonated phosphate groups constitutes 57 of the 58 individual mineral species. The most common of these species is the mineral whitlockite (Fron del, 1941; Hughes et al., 2008), although other examples include brushite, monetite, newberyite, and groatite (Cooper et al., 2009; Duff,

1971; Frost et al., 2011; Terpstra, 1937). Only one mineral species (bobdownsite) is reported to have an essential monofluorophosphate component (PO_3F^{2-}) in its structure.

Bobdownsite was approved as a new mineral by the International Mineralogical Association in 2008 (IMA number 2008-037), and it was described in detail by Tait et al. (2011). The type locality of bobdownsite is in Big Fish River, Yukon Canada. Bobdownsite is also reported to occur at a number of other localities on Earth (e.g., Tip Top Mine, South Dakota USA), and it has been reported in martian meteorites (Gnos et al., 2002; Tait et al., 2011). In addition to bobdownsite, the mineral krásnoite is reported to contain fluorophosphate groups (Mills et al., 2012), but, unlike bobdownsite, the validity of krásnoite as a species is not predicated on the assignment of fluorine to fluorophosphate groups. Although only two naturally occurring fluorophosphate compounds have been reported, there is a wide array of synthetic fluorophosphate compounds that have many versatile uses from additives in toothpaste (Sten, 1964) to treatments for osteoporosis (Balena et al., 1998; Kleerekoper, 1998; Lems et al., 2000). In the present study, we provide in-depth structural and chemical characterization of bobdownsite from the type locality in Big Fish River, Yukon Canada to reassess whether or not fluorine is present, and if so, how it is bonded within the structure. The results of this study will be compared and contrasted with previous studies of bobdownsite, krásnoite, as well as a number of well-characterized synthetic monofluorophosphate salts. The aim of our study is to establish minimum criteria for identifying and classifying minerals with an essential monofluorophosphate structural component.

Methods

Samples analyzed in the present study

Bobdownsite samples from the type locality in Big Fish River, Yukon Canada were obtained from a number of sources: Samples of bobdownsite were personally collected by coauthor

KTT in July, 2012 at the same locality that the bobdownsite type sample was collected at Rapid Creek, Yukon, Canada. The mineral was not found *in situ*, but collected in the talus slope below the original find (samples identified as Bobdownsite_Tait); bobdownsite specimens were purchased from Rod Tyson of Tysons' Fine Minerals Inc. (samples identified as bobdownsite_A); and we also obtained the type specimen of bobdownsite from Robert Downs at the University of Arizona (sample number R050109). In addition, Robert Downs provided us with a sample of bobdownsite from the Tip Top Mine in South Dakota, USA (sample number R070654). Finally, we purchased a sample that was described as whitlockite from Steve Covey of Amethyst Galleries' Mineral Gallery from Big Fish River, Yukon Canada (samples identified as Yukon phosphate) that is identical in appearance to the bobdownsite from the same locality. We suspect that the material is the same as the other material from this locality, which is supported by the fact that the whitlockite specimen was purchased in 2009, prior to the publication of Tait et al. (2011) describing bobdownsite for the first time.

In addition to using the natural samples described above, we also synthesized whitlockite ($\text{Ca}_9\text{Mg}[\text{PO}_3\text{OH}][\text{PO}_4]_6$) (sample identified as MGS-008) to use as a F- and Fe-free standard to compare with the natural bobdownsite samples. The whitlockite synthesis was conducted using the methods of Adcock et al. (2013; 2014), which are optimized after Hughes et al. (2008) and Gopal et al. (1974). A solution containing 90 ml of high-purity (18.2M Ω) water, 1.00 g of laboratory-grade hydroxylapatite (Spectrum, reagent grade) and 0.30 g magnesium nitrate hexahydrate (J.T. Baker, ACS grade) is created in a 125 ml Parr acid digestion vessel (Parr 4748) with an acid-washed polytetrafluoroethylene liner. Once the solution is mixed, it is acidified to a pH of 2.6–2.8 using concentrated phosphoric acid (Alfa Aesar, ACS grade). The vessel is then sealed and incubated in an oven at 240 °C for 7 days. At the end of 7 days, the vessel is removed

from the oven and quenched in a water bath in an effort to prevent any further reaction. After cooling, the vessel is opened and the solution decanted leaving the solids. Solid material is rinsed from the vessel using ethanol, allowed to air dry for 24 h, weighed and inspected by optical microscopy for preliminary phase identification. Additional phases can form during synthesis, typically hydroxylapatite ($\text{Ca}_5[\text{PO}_4]_3\text{OH}$) and monetite (CaHPO_4), but are primarily confined to the $<75\ \mu\text{m}$ fraction. Output masses are therefore brush sieved on a 200 mesh screen to remove the $<75\ \mu\text{m}$ size fraction. The methods have been shown to consistently and reliably produce high-purity Mg-endmember whitlockite (Adcock et al., 2013; Adcock et al., 2017; Hughes et al., 2008), although a few wt.% of merrillite may occur within the whitlockite (Adcock et al., 2017; Hughes et al., 2008).

Electron probe microanalysis (EPMA)

All of the natural phosphate specimens (Bobdownsite_A, Yukon phosphate, Bobdownsite_Tait, R050109, and R070654) were analyzed using the JEOL 8200 electron microprobe at the Institute of Meteoritics at the University of New Mexico using Probe for EPMA™ (PFE) software. An accelerating voltage of 15 kV, a nominal probe current of 20 nA, and a beam diameter of $5\ \mu\text{m}$ were used during each analysis. We analyzed for the elements Si, Al, Fe, Mn, Mg, Ca, Na, P, F, and Cl. F was analyzed using a light-element LDE1 detector crystal, and Cl was analyzed using a PET detector crystal. The standards used were as follows; for Ca and P, Durango apatite (Jarosewich et al., 1980) was used as the primary standard, and a natural fluorapatite from India (Ap020 from McCubbin et al., 2012) was used as a secondary check on the standardization. A synthetic SrF_2 crystal from the Taylor multi element standard mount (C. M. Taylor) was used as the primary F standard, and Ap020 was used as an additional check on the F

standardization. We have demonstrated previously that SrF₂ is a reliable fluorine standard for the analysis of fluorine in both glasses and apatite (McCubbin et al., 2016; McCubbin et al., 2015b). A synthetic sodalite crystal from Sharp et al. (1989) was used as a primary Cl standard, and scapolite from the Smithsonian Institution (NMNH R6600-1) was used as a secondary check on the Cl standardization. Spessartine, albite, and quartz from the Taylor multi element standard mount (C.M. Taylor) were used as primary standards for Mn, Na, and Si, respectively. Pyrope from the Taylor multi element standard mount (C.M. Taylor) was used for Mg and Al. Ilmenite from the Smithsonian Institution (NMNH 133868) was used as a primary standard for Fe.

The synthetic Mg-whitlockite (MGS-008) was analyzed using a JEOL JXA-8900 at the EMiL facility within the University of Nevada, Las Vegas. An accelerating voltage of 15 kV, a nominal probe current of 10 nA, and a beam diameter of 10 μm were used during each analysis. We analyzed for the elements Si, Fe, Mn, Mg, Ca, Na, P, S, and Cl. Cl was analyzed using a PETJ detector crystal. Standards included apatite for Ca from the Smithsonian Institution (NMNH 104021) (Jarosewich, 2002) and San Carlos olivine for Mg and Si. Fe and Mn were standardized using ilmenite sample NMNH 96189. Kakanui anorthoclase was used as a standard for Na, and scapolite NMNH R6600 was used for Cl. P was standardized using Micro-Analysis Consultants Ltd. Apatite from Yates Mine, Quebec (MAC EMS 80095-MINA apatite). S was standardized using Micro-Analysis Consultants Ltd. pyrite, also from Yates Mine, Quebec (MAC EMS 80095-MINA pyrite).

Carbon reduction Gas-chromatography–isotope ratio mass spectrometry

Gas chromatography isotope-ratio mass spectrometry (GC-IRMS) was used to quantify water contents in Bobdownsite_A and Yukon phosphate samples, and H isotopic values were also

determined for the Yukon phosphate sample. Measurements were made in the Center for Stable Isotopes in the Department of Earth and Planetary Sciences at the University of New Mexico, using the technique and apparatus previously described in detail by Sharp et al. (2001). Briefly, the technique involves reduction of structural OH components in the phosphate samples to H₂ gas by reaction with glassy carbon at 1450°C in a helium carrier gas. Product gases are separated in a gas chromatograph and analyzed in a mass spectrometer configured to make hydrogen isotope analyses in continuous flow mode. In the present study, the phosphate samples were wrapped in silver foil and dropped into the furnace using a commercially available autosampler (e.g., Carlo Erba AS 200-LS) mounted directly over the reduction tube. We used sample sizes of about 5–11.5 mg, which produced a sufficient volume of H₂ to quantitatively determine the abundances of H₂O in the phosphates. The detection limits for H₂O during our session were determined by running empty silver foil buckets that were used to wrap the phosphate samples, which yielded a detection limit of approximately 300 ppm H₂O, which is equivalent to approximately 0.006 µl H₂O that we attribute to adsorbed surface water on the silver. This base level amount of adsorbed surface water is consistent with the blank H₂O contents from other investigations using this laboratory (McCubbin et al., 2012). This technique was also used to determine δD values using standard correction procedures, which produced results identical to those obtained conventionally with a precision of 4‰ (2σ) for hydrous minerals that have at least 0.1 µl H₂O (Sharp et al., 2001) (equivalent to 5000 ppm H₂O in the phosphate samples that were analyzed). Throughout our analysis routine, we checked the reproducibility of the column using several H₂O standards including NBS 30 biotite (Sharp et al., 2001), water canyon biotite (USGS sample number 3149-11), and BUD biotite (Bindeman and Serebryakov, 2011). For each phosphate sample, we analyzed four to seven separate aliquots of sample to test for homogeneity in our phosphate grains. Water

contents for the phosphate samples are presented in **Table 1**. The 2σ uncertainty reported in **Table 1** refers to the standard deviation of the mean water contents among all analyses for each sample, which was larger than the analytical uncertainty. Total time of analysis is less than two minutes for a single hydrogen and δD analysis.

Raman Spectroscopy

Raman spectra of Bobdownsite_A and Yukon phosphate were collected using a Witec α -Scanning Near-Field Optical Microscope (SNOM) confocal Raman spectrometer. Both samples were prepared as polished mounts. The excitation source is a frequency-doubled solid-state YAG laser (532 nm) operating between 0.3 and 1 mW output power (dependent on objective), as measured at the sample using a laser power meter. Objective lenses included a x100 LWD and a x20 LWD with a 50 μm optical fiber acting as the confocal pin hole. Spectra were collected on a Peltier-cooled Andor EMCCD chip, after passing through a f/4 300 mm focal length imaging spectrometer typically using a 600 lines/mm grating. The lateral resolution of the instrument is as small as 360 nm in air when using the x100 LWD objective, with a focal plane depth of ~ 800 nm.

We employed this instrument to collect single spectra of the Bobdownsite_A and Yukon phosphate samples. Single spectra mode allows the acquisition of a spectrum from a single spot on the target. Average spectra are produced using integration times of 30 seconds per accumulation and 10 accumulations to allow verification of weak spectral features. A cosmic ray reduction routine was used to reduce the effects of stray radiation on Raman spectra.

Nuclear Magnetic Resonance (NMR) spectroscopy

NMR spectra were collected on Bobdownsite_A, Yukon phosphate, and the synthetic Mg-whitlockite sample, MGS-008. The ^{19}F single-pulse (SP) spectra were collected on a 500 MHz (11.7 T) Varian InfinityPlus spectrometer operating at 470.179 MHz, using a Varian/Chemagnetics T3-type probe assembly configured for 3.2 mm (O.D.) rotors. The 90° pulse width was $5\mu\text{s}$, and 170 transients were collected at a relaxation delay of 100s. Longer relaxation delays produced nominal increases in signal, however the NMR lineshapes did not change at relaxation delays up to 600s. Chemical shifts were measured relative to neat CFCl_3 set to $\delta_{\text{F}} = 0$ ppm. The MAS rate was 20 kHz. Additional spectra were acquired after a small amount of NaF was added to each sample, corresponding approximately to one F per formula unit (i.e., an F:P ratio of 1:7). The ^1H SP/MAS spectra were collected on a 400 MHz (9.4T) Varian Inova spectrometer operating at 399.895 MHz. A probe assembly modified for low ^1H background and configured 4 mm (O.D.) rotors was used, with the samples contained in ZrO_2 rotors having Kel-F tips, and PTFE spacers. The MAS rate was 10 kHz. The 90° pulse width was $5\mu\text{s}$ with a pulse delay of 30 seconds, and 128 transients were collected. Chemical shifts were measured relative to hydroxylapatite set to $\delta_{\text{H}} = 0.2$ ppm. The ^{31}P NMR spectra were acquired with the 500 MHz spectrometer and a T3-type probe fitted with 4 mm spinning assembly and at a 15 kHz spinning rate. The single-pulse spectra were collected with $4\mu\text{s}$ pulses, where the 90° pulse width was $5\mu\text{s}$. For the synthetic samples, spectra collected fully relaxed as a single acquisition after overnight equilibration did not differ significantly from spectra acquired with a 300 s relaxation delay. The ^{31}P chemical shifts are referenced to 85% H_3PO_4 , set to $\delta_{\text{P}} = 0$ ppm.

Results

Chemical and isotopic composition of phosphates

The compositions of all the phosphates analyzed in the present study are provided in **Table 1**, and the H₂O abundances of samples Bobdownsite_A and Yukon phosphate are also provided in **Table 1**. All of the phosphates from Big Fish River, Yukon, Canada have similar compositions with some variations in Na, Mg, and Fe (**Table 1**). Sodium abundances in these samples range from 0.61 to 1.00 wt.% Na₂O, which corresponds to 0.21–0.34 structural formula units of Na (sfu) per 28 oxygens. Fe and Mg abundances in the samples from Big Fish River are inversely correlated and range from 1.08 to 1.43 wt.% FeO and 2.63 to 2.88 wt.% MgO. These abundances correspond to 0.16 to 0.21 sfu Fe and 0.69 to 0.73 sfu Mg per 28 oxygens. The sum of Fe and Mg per 28 oxygens ranges from 0.90 to 0.94 sfu. Although H₂O abundances were only measured in the samples Bobdownsite_A and Yukon phosphate, they yielded similar results of 0.71 and 0.70 wt.% H₂O, respectively. These abundances of H₂O correspond to 0.83 to 0.86 sfu OH per 28 oxygens. Fluorine was not detected in any of the phosphates analyzed in the present study, so the chemistry of the phosphates indicate that they are whitlockite with compositions that lie along the whitlockite-merrillite solid solution.

The sample from the Tip Top mine, South Dakota, USA (R070654) was distinctly different from the samples from Big Fish River, Yukon, Canada given the paucity of FeO, lower abundance of Na, and elevated abundance of Mg (**Table 1**). We did not detect any fluorine within sample R070654, so it is also likely a phase that lies along the whitlockite-merrillite solid solution; however direct analysis of H₂O is required to definitively identify the sample as either whitlockite or merrillite. The synthetic sample MGS-008 is an endmember Mg-whitlockite and does not have detectable Fe or Na (**Table 1**).

In addition to elemental abundances, we measured the H-isotopic composition of the sample Yukon phosphate. Isotopic compositions are traditionally expressed in delta notation according to the following equation:

$$\delta^M X = \left[\frac{\frac{Heavy^M X_{Measured}}{Light^M X_{Measured}} \times \frac{Light^M X_{Standard}}{Heavy^M X_{Standard}}}{\frac{Light^M X_{Measured}}{Heavy^M X_{Standard}}} - 1 \right] \times 1000 \quad (1)$$

where $\frac{Heavy^M X_{Measured}}{Light^M X_{Measured}}$ is the isotopic ratio of the measured sample, $\frac{Light^M X_{Standard}}{Heavy^M X_{Standard}}$ is the isotopic ratio of the standard, and $\delta^M X$ is the delta value of the isotope expressed in per mil. The standard for D/H is Vienna Standard Mean Ocean Water with D/H of 1.5576×10^{-4} (Coplen, 1994). The H isotopic composition of the sample Yukon phosphate has a D value of $-200 \pm 12\%$, which is similar to meteoric waters in northern Yukon Canada where the samples originated (e.g., Tondu et al., 2013), and it is distinct from meteoric waters in Albuquerque, NM where the samples were analyzed and stored prior to analysis (e.g., Yapp, 1985).

Raman Spectroscopy

We analyzed the samples Bobdownsite_A and Yukon phosphate by Raman spectroscopy, and Raman spectra for samples R050109 and R070654 were reported by Tait et al. (2011). Spectra from all four samples are displayed in **Figure 1**. All spectra exhibit the same patterns, consistent with being comprised of similar material. Peaks in the range of 900 to 1180 cm^{-1} are associated with P-O vibrations (Socrates, 2001). The most prominent peak in this region is represented by the symmetric P-O stretch (ν_1) in phosphate at $\sim 970 \text{ cm}^{-1}$. The broad weak peaks in the range of 1070-1120 cm^{-1} are representative of the asymmetric P-O stretching (ν_3) in phosphate. The sharp

medium to weak intensity peak at approximately 923-925 cm^{-1} is in the region that has been attributed to the symmetric stretching mode (ν_1) of HPO_4^{2-} in whitlockite (Jolliff et al., 2006). We observe no peaks in the region of the symmetric P-F stretching mode (ν_1) of 776 to 840 cm^{-1} range (highlighted in gray in Figure 1) reported previously for the P-F symmetric stretch (ν_1) in PO_3F^{2-} from monofluorophosphate salts (Baran and Weil, 2009; Weil et al., 2015; Weil et al., 2007).

^{19}F and ^1H NMR

^{19}F is the second most sensitive naturally occurring stable nuclide for NMR spectroscopy, with a detection limit estimated to be of the order 100 $\mu\text{g F g}^{-1}$, but no ^{19}F MAS/NMR signal was detected from the Bobdownsite_A, Yukon phosphate, and synthetic whitlockite (MGS-008) samples. To check this result, additional spectra were acquired after addition of small amounts of NaF (4.5–6 wt. percent), equivalent to approximately one F per formula unit (i.e., an F:P ratio of 1:7). Spectra acquired after addition of the NaF contain a central peak at $\delta_{\text{F}} = -220$ ppm and associated spinning sidebands (Fig. 2), but no other signals. This chemical shift is in good agreement with previous reports for NaF (Stebbins and Zeng, 2000). Previous ^{19}F NMR studies of inorganic fluorophosphate compounds show spectra containing wide spinning sideband manifolds with distinct center band doublets for the fluorophosphate F. The ^{19}F chemical shifts for the fluorophosphate group range from -52.5 ppm for BaPOF_3 to -75 ppm for $\text{Na}_2\text{PO}_3\text{F}$ (Jantz et al., 2016; Stoeger et al., 2013; Weil et al., 2004; Weil et al., 2007; Zhang et al., 2007). No signal in this chemical shift range (shaded region of Fig. 2) occurs in the spectra of the Bobdownsite_A and Yukon phosphate samples from Big Fish River, Yukon Canada.

The synthetic whitlockite sample yields a well-resolved, relatively narrow ^1H NMR peak near $\delta_{\text{H}} = +10$ ppm (Fig. 3), consistent with the presence of a single hydrogen phosphate group in

the crystal structure. Additional minor signals occur near +7 ppm and +12 ppm, possibly from unidentified impurities. The ^1H NMR spectra of the natural Bobdownsite_A and Yukon phosphate samples also contain a major peak centered near +10 ppm, although the peaks are significantly broader and exhibit substantially more spinning sideband intensity than the synthetic whitlockite. The broader resonances likely result from minor concentrations of paramagnetic ions in the mineral specimens (e.g., Begaudeau et al., 2012; Oldfield et al., 1983), consistent with the 1.1 to 1.4 wt.% FeO in these samples (Table 1). An additional minor peak occurs in the synthetic whitlockite near +0.2 ppm that can be attributed to an impurity phase, possibly hydroxylapatite based on its similar chemical shift (Yesinowski and Eckert, 1987).

^{31}P NMR

The ^{31}P MAS/NMR spectra of the Bobdownsite_A and Yukon phosphate specimens contain broad, poorly resolved centerbands centered near +0.6 ppm, 5.5 ppm FWHM (Fig. 4). In contrast, the synthetic whitlockite (MGS-008) sample yields well-resolved centerbands exhibiting sharp peaks at 2.3, 1.4, and -0.2 ppm plus shoulders at +0.7 and -0.8 ppm. Minor additional peaks occur at -3.4 and -4.3 ppm that could arise from impurity phases. Qualitatively, the centers of gravity of the Bobdownsite_A and Yukon phosphate spectra coincide with that of the synthetic whitlockite (MGS-008). This result suggests that peak broadening by paramagnetic substituents present in the natural samples, similar to that discussed for the ^1H results above, prevents resolution of distinct sites. However, the spectrum of the natural Yukon phosphate sample does appear to exhibit an asymmetry that suggests the presence of at least two peaks at positions similar to those for the main peaks for the synthetic sample, namely at +2.3 and -0.2 ppm. The chemical shifts for the main peaks observed for these samples lie well within ranges reported previously for

orthophosphate groups in general, and Ca- and Mg-orthophosphates in particular (Belton et al., 1988; Rothwell et al., 1980; Turner et al., 1986).

The spectrum of the synthetic whitlockite (MGS-008) is consistent with the presence of three crystallographically distinct P positions in a 3:1:3 ratio plus additional signals arising from merrillite-like local environments (Calvo and Gopal, 1975). A more complete report of the NMR spectra of whitlockite and assignment of the resolved features will be presented in a separate paper.

Discussion

Discreditation of bobdownsite

Based on the similarities in chemical composition and the nearly identical Raman spectra among all phosphate samples analyzed from Big Fish River, Yukon Canada, we infer that all samples from this locality are comprised of the same mineral phase. Consequently, we refer to all of these samples collectively as “bobdownsite” throughout the discussion except in cases where we refer to a specific sample, in which case the sample name is used.

Three of the primary lines of evidence that supported the identification of bobdownsite require reassessment based on differences in results between the present study and the initial description of this mineral (i.e., Tait et al., 2011). These include the absence of OH⁻ in the samples inferred by thermogravimetric analysis (TGA), the assignment of a Raman peak at 923 cm⁻¹ to symmetric stretching in PO₃F²⁻, and the abundance of fluorine determined by EPMA. We will first compare data from Tait et al. (2011) and the present study and then use NMR results from the present study to resolve any remaining discrepancies.

H abundance of “bobdownsite”

Samples of “bobdownsite” heated to 1100 °C by Tait et al. (2011) did not exhibit weight loss that could be attributed to the presence of OH in the structure. However, in the present study, “bobdownsite” was heated to 1450 °C and H was liberated from the sample, yielding approximately 0.7 ± 0.05 wt.% H₂O with an H isotopic composition of -200 ± 12 ‰. The abundance of H₂O fills the equivalent of at least 83% of the OH⁻-site in whitlockite with OH⁻. The presence of OH⁻ in the “bobdownsite” structure is confirmed by our observation of ¹H NMR signals for a hydrogen phosphate group in samples from the Big Fish River, Yukon Canada locality.

Vibrational spectroscopy of “bobdownsite”

The fluorophosphate group occurs in a number of inorganic salts for which crystal structures and vibrational spectra have been reported (Baran and Weil, 2009; Heide et al., 1985; Jantz et al., 2016; Weil et al., 2015; Weil et al., 2004; Weil et al., 2007; Zeibig et al., 1991). Owing to a lack of significant bonding of fluorine beyond the P-F bond in most of these compounds, the P-F stretching frequency is typically observed to vary only slightly from its value for aqueous fluorophosphate ion, 795 cm⁻¹ (Siebert, 1966). A small variation in the symmetric P-F stretching mode has been observed, ranging from 776 cm⁻¹ to 840 cm⁻¹ that in some cases appears to relate to the P-F bond distance (Baran and Weil, 2009; Heide et al., 1985; Jantz et al., 2016; Weil et al., 2015; Weil et al., 2004; Weil et al., 2007; Zeibig et al., 1991). The wavenumber range of stretching modes attributed to P-F bonds in fluorophosphate salts falls outside that typical for the symmetric P-O stretch in phosphate and hydrogen phosphate. In contrast, Tait et al. (2011) analyzed bobdownsite by Raman spectroscopy, assigning a peak at 923 cm⁻¹ to the P-F ν_1 mode in PO₃F²⁻. However, 923 cm⁻¹ falls outside the range reported for P-F symmetric stretching modes exhibited

by synthetic fluorophosphate salts (Baran and Weil, 2009; Heide et al., 1985; Jantz et al., 2016; Weil et al., 2015; Weil et al., 2004; Weil et al., 2007; Zeibig et al., 1991). Our analyses of bobdownsite_A and Yukon phosphate match those of Tait et al. (2011) for samples R050109 and R070654, which supports the argument that a fluorophosphate group attributed to “bobdownsite” is misidentified (Figure 1), despite the fact that the refined P-F bond distance from the XRD results of Tait et al. (2011) falls within the range of crystalline fluorophosphate salts (although substantially longer than previous reports for all except $\text{NaK}_3(\text{PO}_3\text{F})_2$; Durand et al., 1975). Finally, the Raman spectra of the purported “bobdownsite” specimens are strikingly similar to those reported for a whitlockite specimen from the Palermo type locality (R080052) in Tait et al. (2011), which also exhibits a peak at about 923 cm^{-1} . Peaks in vibrational spectra near 923 cm^{-1} have been attributed in previous studies to the P-O stretch for the hydroxyl oxygen in the hydrogen phosphate group (e.g., Jolliff et al., 2006; Socrates, 2001). Assignment of the 923 cm^{-1} peak to the P-O(H) vibration is consistent with our observation of ^1H NMR signals for a hydrogen phosphate group in samples from these localities.

F abundance of “bobdownsite”

Although Tait et al. (2011) reported fluorine abundances by EPMA in samples R050109 and R070654 of 1.9 and 1.5 wt.% F, respectively, fluorine was below detection (detection limit was approximately 0.05 wt.% F) in our EPMA analyses of R050109 and R070654 as well as the other phosphate samples from Big Fish River, Yukon Canada that we analyzed. To accurately measure fluorine by EPMA, a synthetic multilayer crystal with a large d-spacing (e.g., LDE-1, OV-60, PC0) is typically preferred over the more classically used and widely available thallium acid phosphate (TAP) crystal because the intensity of the F $K\alpha$ peak using the multilayer crystal

is approximately 14 times higher than with TAP (Potts and Tindle, 1989; Raudsepp, 1995; Reed, 2005). This enhanced intensity in the F K α line renders the interference from a third order P K α line (and all other third order or greater interferences) on the F K α line insignificant, which was one of the primary problems with analyzing F in apatite using a TAP crystal (Potts and Tindle, 1989; Raudsepp, 1995; Reed, 2005). Furthermore, the primary difference in the EPMA routines between our study and that of Tait et al. (2011) is our use of an LDE-1 crystal to measure fluorine X-ray counts versus use by Tait et al. (2011) of a TAP crystal (Robert Downs Pers. Comm.); this may explain the differences between our results. We further investigated whether or not F was present in the “bobdownsite” using ^{19}F MAS/NMR spectroscopy, which confirmed that F was below detection (~ 100 ppm F) in the “bobdownsite” samples, consistent with our EPMA results.

Whitlockite from Big Fish River, Yukon Canada

The mineral “bobdownsite” is differentiated from whitlockite based on the presence of a monofluorophosphate group (PO_3F^{2-}) rather than a protonated phosphate group ($\text{PO}_3\text{OH}^{2-}$). We were unable to detect fluorine in any of the phosphate specimens from Big Fish River, Yukon Canada, including the type specimen R050904. Furthermore, measured H_2O abundances were at a level consistent with a whitlockite along the whitlockite-merrillite join. Consequently, we regretfully conclude that the mineral bobdownsite must be discredited.

Implications for structural accommodation of fluorine in krásnoite

The mineral krásnoite [$\text{Ca}_3\text{Al}_{7.7}\text{Si}_3\text{P}_4\text{O}_{22.9}(\text{OH})_{13.3}\text{F}_2 \cdot 8\text{H}_2\text{O}$] is reported to be the fluorine analog of the mineral perhamite (Mills et al., 2011). In a follow-up manuscript describing the mineral krásnoite, Mills et al. (2012) concluded that the fluorine was substituting for OH^- on a

hydrogen phosphate anion ($\text{PO}_3\text{OH}^{2-}$), forming a fluorophosphate group rather than substituting for one of the other OH^- sites available in the mineral. Although krásnoite is a valid species regardless of the structural accommodation mechanism of fluorine, we have examined the assignment of fluorine to a monofluorophosphate component given the paucity of such molecular groups in other minerals as exemplified by the discreditation of bobdownsite. There are two primary lines of evidence used by Mills et al. (2012) to support the occurrence of monofluorophosphate groups in krásnoite, including vibrational (Raman and IR) spectroscopic data and ^{19}F MAS NMR data. We compare the data in Mills et al. (2012) with those published on synthetic monofluorophosphate salts to further elucidate the structural role of F in krásnoite.

Mills et al. (2012) also reported both Raman and FTIR data for krásnoite. They assigned a Raman peak at 920 cm^{-1} to the P-F symmetric stretching mode in PO_3F based on the same assignment in bobdownsite from Tait et al. (2011); however, this peak position falls outside the range of the F-P ν_1 mode in PO_3F from fluorophosphates salts (Baran and Weil, 2009; Heide et al., 1985; Jantz et al., 2016; Weil et al., 2015; Weil et al., 2004; Weil et al., 2007; Zeibig et al., 1991), instead falling within the range of stretching and bending modes attributed to P-O or P-O(H) groups (Jolliff et al., 2006; Socrates, 2001). Therefore, the 920 cm^{-1} Raman peak is likely not indicative of a monofluorophosphate group in krásnoite. A peak at 820 cm^{-1} within the FTIR spectrum of krásnoite was also assigned to a fluorophosphate group by Mills et al. (2012). The position of the P-F ν_1 modes for fluorophosphate salts ranges from 727 to 824 cm^{-1} (Baran and Weil, 2009; Jantz et al., 2016; Weil et al., 2015; Weil et al., 2004; Weil et al., 2007), so the assignment of a P-F ν_1 mode to the 820 cm^{-1} in krásnoite is permissive; nevertheless, the lack of a corresponding Raman peak to corroborate this assignment does not lend confidence to the interpretation, especially given overlaps in the 820 cm^{-1} region with a number of other peaks

related to Al-O or Si-O vibrational modes (Socrates, 2001). Consequently, the vibrational spectroscopic data do not provide sufficient evidence that krásnoite contains monofluorophosphate groups within its structure.

Mills et al. (2012) reported ^{19}F MAS NMR results for krásnoite that were interpreted to verify the presence of F in the mineral structure. Because chemical shifts reported by Mills et al. (2012) were relative to CaF_2 , we have converted their values relative to CFCl_3 , the conventional standard for ^{19}F NMR spectral comparisons (e.g., Huve et al., 1992). The chemical shift of ^{19}F in CaF_2 relative to CFCl_3 is -110 ppm (Wang and Grey, 1998), which corresponds to a new primary peak at a chemical shift of -130 ppm with minor peaks at chemical shifts of -110 ppm, -140 ppm, and -150 ppm. The ^{19}F chemical shifts for the monofluorophosphate groups in fluorophosphate salts ranges from -52.5 ppm for BaPOF_3 to -75 ppm for $\text{Na}_2\text{PO}_3\text{F}$ (Jantz et al., 2016; Stoeger et al., 2013; Weil et al., 2004; Weil et al., 2007; Zhang et al., 2007), which are substantially displaced from the observed ^{19}F chemical shifts for krásnoite (Mills et al., 2012). Consequently, the ^{19}F MAS NMR data in Mills et al. (2012) do not support assignment of F in krásnoite to monofluorophosphate groups. Furthermore, the ^{19}F NMR peak for monofluorophosphate should be represented by a doublet owing to the strong scalar coupling between ^{19}F and ^{31}P nuclei (e.g., Stoeger et al., 2013). In addition, Mills et al. (2012) attributed the peak at a chemical shift of -150 ppm to a minor fluorapatite impurity, whereas ^{19}F NMR spectra of fluorapatite exhibit a chemical shift near -103 ppm (e.g., Braun et al., 1995; Mason et al., 2009; McCubbin et al., 2008), which is not exhibited by the ^{19}F NMR spectra for krásnoite. To further elucidate the role of F in the structure of krásnoite, we have interpreted the ^{19}F NMR spectra accordingly and show that the chemical shifts observed at -130, -140, and -150 ppm can be ascribed to Al-F groups (Chupas et

al., 2003; Kao and Chen, 2003; Kiczinski and Stebbins, 2002; Zhang et al., 2002), indicating that F⁻ likely substitutes for OH⁻ bonded to Al in perhamite (i.e., Mills et al., 2006).

Proposed criteria for identification of minerals with a monofluorophosphate (PO₃F²⁻) anion

We recommend that future reports of new minerals containing essential monofluorophosphate anions be vetted by abundance measurements of fluorine, vibrational spectroscopy (both Raman and FTIR), and where paramagnetic components are permissibly low, NMR spectroscopy. Furthermore, the previous reports of bobdownsite and krásnoite highlight the importance of using synthetic compounds containing monofluorophosphate anions as a point of comparison in the identification of minerals with essential monofluorophosphate. Given that fluoride is a common substituent for hydroxyl in many phosphates and occupies crystallographic sites in phosphates that are not bonded directly to phosphorus, a concerted effort should also be made to verify that a proposed new monofluorophosphate mineral contains PO₃F molecular groups, or at minimum, P-F bonds. Although not a shortcoming of the bobdownsite and krásnoite studies (Mills et al., 2012; Tait et al., 2011), it must be emphasized that structural data that yield satisfactory P-F bond lengths determined by X-ray crystallography, coupled with direct chemical analyses of fluorine in a material, do not constitute sufficient evidence alone to identify a new mineral having essential monofluorophosphate anions.

Implications

The preponderance of data collection on whitlockite from Big Fish River, Yukon Canada has highlighted the potential utility of this material as a phosphate standard for H abundance and H-isotopic analysis by secondary ion mass spectrometry (SIMS). Given the heightened interest in

the analysis of hydrogen abundances and hydrogen isotopes in phosphates from planetary materials (i.e., Barnes et al., 2013; Barnes et al., 2014; Barrett et al., 2016; Boctor et al., 2003; Boyce et al., 2012; Boyce et al., 2010; Greenwood et al., 2008; Greenwood et al., 2011; Jones et al., 2014; Jones et al., 2016; Mane et al., 2016; McCubbin et al., 2012; McCubbin et al., 2014; McCubbin et al., 2010; Robinson et al., 2016; Robinson and Taylor, 2014; Sarafian et al., 2014; Sarafian et al., 2013; Tartèse et al., 2013; Tartèse et al., 2014a; Tartèse et al., 2014b; Treiman et al., 2014), the identification of whitlockite with consistent inter- and intra-granular H₂O abundances and an isotopically light H isotope composition is unique among available phosphate SIMS standards (c.f., McCubbin et al., 2015a, and references therein). Given that many of the SIMS analyses of merrillite in planetary samples have been conducted using apatite standards (Mane et al., 2016; McCubbin et al., 2014), a whitlockite standard will provide a better matrix match for future SIMS studies of merrillite or whitlockite in Earth and planetary materials.

Acknowledgments

We thank Angela Garcia for help with mineral synthesis. We thank the International Mineralogical Association (IMA) Commission on New Minerals, Nomenclature, and Classification (CNMNC) for consideration and approval of our proposal to discredit bobdownsite (Proposal # 17-E). We are grateful to the Aaron Celestian for the editorial handling of the manuscript and we are thankful to Matthew Pasek and Guy Hovis for constructive reviews that improved the quality of the manuscript. This work was partially supported by a NASA Mars Fundamental Research grant awarded to FMM. Additionally, NMR spectroscopic analyses at Stony Brook University were supported by NSF grant EAR 1249696 awarded to BLP.

References

Adcock, C.T., Hausrath, E.M. and Forster, P.M. (2013) Readily available phosphate from minerals in early aqueous environments on Mars. *Nature Geoscience*, 6, 824–827.

- Adcock, C.T., Hausrath, E.M., Forster, P.M., Tschauner, O. and Sefein, K.J. (2014) Synthesis and characterization of the Mars-relevant phosphate minerals Fe- and Mg-whitlockite and merrillite and a possible mechanism that maintains charge balance during whitlockite to merrillite transformation. *American Mineralogist*, 99, 1221–1232.
- Adcock, C.T., Tschauner, O., Hausrath, E.M., Udry, A., Luo, S.N., Cai, Y., Ren, M., Lanzirotti, A., Newville, M., Kunz, M. and Lin, C. (2017) Shock-transformation of whitlockite to merrillite and the implications for meteoritic phosphate. *Nature Communications*, 8, 14667 doi: 10.1038/ncomms14667.
- Balena, R., Kleerekoper, M., Foldes, J.A., Shih, M.S., Rao, D.S., Schober, H.C. and Parfitt, A.M. (1998) Effects of different regimens of sodium fluoride treatment for osteoporosis on the structure, remodeling and mineralization of bone. *Osteoporosis International*, 8, 428–435.
- Baran, E.J. and Weil, M. (2009) Vibrational spectra of the layered monofluorophosphate (V), $\text{NH}_4\text{Ag}_3(\text{PO}_3\text{F})_2$. *Journal of Raman Spectroscopy*, 40, 1698–1700.
- Barnes, J.J., Franchi, I.A., Anand, M., Tartèse, R., Starkey, N.A., Koike, M., Sano, Y. and Russell, S.S. (2013) Accurate and precise measurements of the D/H ratio and hydroxyl content in lunar apatites using NanoSIMS. *Chemical Geology*, 337–338, 48–55.
- Barnes, J.J., Tartèse, R., Anand, M., McCubbin, F.M., Franchi, I.A., Starkey, N.A. and Russell, S.S. (2014) The origin of water in the primitive Moon as revealed by the lunar highlands samples. *Earth and Planetary Science Letters*, 390, 244–252.
- Barrett, T.J., Barnes, J.J., Tartèse, R., Anand, M., Franchi, I.A., Greenwood, R.C., Charlier, B.L.A. and Grady, M.M. (2016) The abundance and isotopic composition of water in eucrites. *Meteoritics & Planetary Science*, 51, 1110–1124.
- Begaudeau, K., Morizet, Y., Florian, P., Paris, M. and Mercier, J.C. (2012) Solid-state NMR analysis of Fe-bearing minerals: implications and applications for Earth sciences. *European Journal of Mineralogy*, 24, 535–550.
- Belton, P.S., Harris, R.K. and Wilkes, P.J. (1988) Solid-state ^{31}P NMR studies of synthetic inorganic calcium phosphates. *Journal of Physics and Chemistry of Solids*, 49, 21–27.
- Bindeman, I.N. and Serebryakov, N.S. (2011) Geology, Petrology and O and H isotope geochemistry of remarkably ^{18}O depleted Paleoproterozoic rocks of the Belomorian Belt, Karelia, Russia, attributed to global glaciation 2.4 Ga. *Earth and Planetary Science Letters*, 306, 163–174.
- Boctor, N.Z., Alexander, C.M.O., Wang, J. and Hauri, E. (2003) The sources of water in martian meteorites: Clues from hydrogen isotopes. *Geochimica et Cosmochimica Acta*, 67, 3971–3989.
- Boyce, J.W., Eiler, J.M. and Channon, M.B. (2012) An inversion-based self-calibration for SIMS measurements: Application to H, F, and Cl in apatite. *American Mineralogist*, 97, 1116–1128.
- Boyce, J.W., Liu, Y., Rossman, G.R., Guan, Y., Eiler, J.M., Stolper, E.M. and Taylor, L.A. (2010) Lunar apatite with terrestrial volatile abundances. *Nature*, 466, 466–469.
- Braun, M., Hartmann, P. and Jana, C. (1995) ^{19}F and ^{31}P NMR spectroscopy of calcium apatites. *Journal of Materials Science-Materials in Medicine*, 6, 150–154.
- Calvo, C. and Gopal, R. (1975) Crystal structure of whitlockite from Palmero Quarry. *American Mineralogist*, 60, 120–133.
- Chew, D.M. and Spikings, R.A. (2015) Geochronology and thermochronology using apatite: Time and temperature, lower crust to surface. *Elements*, 11, 189–194.

- Chupas, P.J., Corbin, D.R., Rao, V.N.M., Hanson, J.C. and Grey, C.P. (2003) A combined solid-state NMR and diffraction study of the structures and acidity of fluorinated aluminas: Implications for catalysis. *Journal of Physical Chemistry B*, 107, 8327–8336.
- Cooper, M.A., Hawthorne, F.C., Ball, N.A., Ramik, R.A. and Roberts, A.C. (2009) Groatite, $\text{NaCaMn}^{2+}_2(\text{PO}_4)[\text{PO}_3(\text{OH})]_2$, a new mineral species of the alluaudite group from the tanco pegmatite, Bernic Lake, Manitoba, Canada: Description and crystal structure. *Canadian Mineralogist*, 47, 1225–1235.
- Coplen, T.B. (1994) Reporting of stable hydrogen, carbon, and oxygen isotopic abundances. *Pure and Applied Chemistry*, 66, 273–276.
- Duff, E.J. (1971) Orthophosphates. Part II. The transformations brushite \rightarrow fluoroapatite and monetite \rightarrow fluoroapatite in aqueous potassium fluoride solution. *Journal of the Chemical Society A: Inorganic, Physical, Theoretical*, 0, 33–38.
- Durand, J., Granier, W., Cot, L. and Galigne, J.L. (1975) Structural studies of oxyfluoride compounds of P^{V} . III: Crystal Structure of $\text{NaK}_3(\text{PO}_3\text{F})_2$. *Acta Crystallographica Section B-Structural Science*, 31, 1533–1535.
- Fron del, C. (1941) Whitlockite a new calcium phosphate, $\text{Ca}_3(\text{PO}_4)_2$. *American Mineralogist*, 26, 145–152.
- Frost, R.L., Palmer, S.J. and Pogson, R.E. (2011) Raman spectroscopy of newberyite $\text{Mg}(\text{PO}_3\text{OH}) \cdot 3\text{H}_2\text{O}$: A cave mineral. *Spectrochimica Acta Part a-Molecular and Biomolecular Spectroscopy*, 79, 1149–1153.
- Gnos, E., Hofmann, B., Franchi, I.A., Al-Kathiri, A., Hauser, M. and Moser, L. (2002) Sayh al Uhaymir 094: A new martian meteorite from the Oman desert. *Meteoritics & Planetary Science*, 37, 835–854.
- Gopal, R., Calvo, C., Ito, J. and Sabine, W.K. (1974) Crystal structure of synthetic Mg-whitlockite, $\text{Ca}_{18}\text{Mg}_2\text{H}_2(\text{PO}_4)_{14}$. *Canadian Journal of Chemistry-Revue Canadienne de Chimie*, 52, 1155–1164.
- Greenwood, J.P., Itoh, S., Sakamoto, N., Vicenzi, E.P. and Yurimoto, H. (2008) Hydrogen isotope evidence for loss of water from Mars through time. *Geophysical Research Letters*, 35.
- Greenwood, J.P., Itoh, S., Sakamoto, N., Warren, P., Taylor, L. and Yurimoto, H. (2011) Hydrogen isotope ratios in lunar rocks indicate delivery of cometary water to the Moon. *Nature Geoscience*, 4, 79–82.
- Harlov, D.E. (2015) Apatite: A fingerprint for metasomatic processes. *Elements*, 11, 171–176.
- Hawthorne, F.C. (1998) Structure and chemistry of phosphate minerals. *Mineralogical Magazine*, 62, 141–164.
- Hazen, R.M., Hystad, G., Downs, R.T., Golden, J.J., Pires, A.J. and Grew, E.S. (2015) Earth's "missing" minerals. *American Mineralogist*, 100, 2344–2347.
- Heide, K., Menz, D.H., Schmidt, C. and Kolditz, L. (1985) On the thermal decomposition of $\text{CaPO}_3\text{F} \cdot \text{H}_2\text{O}$. *Zeitschrift Fur Anorganische Und Allgemeine Chemie*, 520, 32–38.
- Hughes, J.M., Jolliff, B.L. and Gunter, M.E. (2006) The atomic arrangement of merrillite from the Fra Mauro Formation, Apollo 14 lunar mission: The first structure of merrillite from the Moon. *American Mineralogist*, 91, 1547–1552.
- Hughes, J.M., Jolliff, B.L. and Rakovan, J. (2008) The crystal chemistry of whitlockite and merrillite and the dehydrogenation of whitlockite to merrillite. *American Mineralogist*, 93, 1300–1305.
- Hughes, J.M. and Rakovan, J.F. (2015) Structurally robust, chemically diverse: Apatite and apatite supergroup minerals. *Elements*, 11, 165–170.

- Huve, L., Delmotte, L., Martin, P., Ledred, R., Baron, J. and Saehr, D. (1992) ^{19}F MAS-NMR study of structural fluorine in some natural and synthetic 2:1 layer silicates. *Clays and Clay Minerals*, 40, 186–191.
- Jantz, S.G., van Wullen, L., Fischer, A., Libowitzky, E., Baran, E.J., Weil, M. and Hoppe, H.A. (2016) Syntheses, Crystal Structures, NMR Spectroscopy, and Vibrational Spectroscopy of $\text{Sr}(\text{PO}_3\text{F}) \cdot \text{H}_2\text{O}$ and $\text{Sr}(\text{PO}_3\text{F})$. *European Journal of Inorganic Chemistry*, 1121–1128.
- Jarosewich, E. (2002) Smithsonian Microbeam Standards. *Journal of Research of the National Institute of Standards and Technology*, 107, 681–685.
- Jarosewich, E., Nelen, J.A. and Norberg, J.A. (1980) Reference samples for electron microprobe analysis. *Geostandards Newsletter*, 4, 43–47.
- Jolliff, B.L., Haskin, L.A., Colson, R.O. and Wadhwa, M. (1993) Partitioning in REE-saturating minerals - theory, experiment, and modeling of whitlockite, apatite, and evolution of lunar residual magmas. *Geochimica et Cosmochimica Acta*, 57, 4069–4094.
- Jolliff, B.L., Hughes, J.M., Freeman, J.J. and Zeigler, R.A. (2006) Crystal chemistry of lunar merrillite and comparison to other meteoritic and planetary suites of whitlockite and merrillite. *American Mineralogist*, 91, 1583–1595.
- Jones, R.H., McCubbin, F.M., Dreeland, L., Guan, Y.B., Burger, P.V. and Shearer, C.K. (2014) Phosphate minerals in LL chondrites: A record of the action of fluids during metamorphism on ordinary chondrite parent bodies. *Geochimica et Cosmochimica Acta*, 132, 120–140.
- Jones, R.H., McCubbin, F.M. and Guan, Y. (2016) Phosphate minerals in the H group of ordinary chondrites, and fluid activity recorded by apatite heterogeneity in the Zag H3-6 regolith breccia. *American Mineralogist*, 101, 2452–2467.
- Kao, H.M. and Chen, Y.C. (2003) ^{27}Al and ^{19}F solid-state NMR studies of zeolite H- β dealuminated with ammonium hexafluorosilicate. *Journal of Physical Chemistry B*, 107, 3367–3375.
- Kendrick, E., Islam, M.S. and Slater, P.R. (2007) Developing apatites for solid oxide fuel cells: insight into structural, transport and doping properties. *Journal of Materials Chemistry*, 17, 3104–3111.
- Kiczanski, T.J. and Stebbins, J.F. (2002) Fluorine sites in calcium and barium oxyfluorides: ^{19}F NMR on crystalline model compounds and glasses. *Journal of Non-Crystalline Solids*, 306, 160–168.
- Kleerekoper, M. (1998) The role of fluoride in the prevention of osteoporosis. *Endocrinology and Metabolism Clinics of North America*, 27, 441–452.
- Lems, W.F., Jacobs, J.W.G. and Bijlsma, J.W.J. (2000) Fluoride in the prevention and treatment of glucocorticoid-induced osteoporosis. *Clinical and Experimental Rheumatology*, 18, S65–S68.
- Lin, J.H., Lou, C.W., Chang, C.H., Chen, Y.S., Lin, G.T. and Lee, C.H. (2007) In vitro study of bone-like apatite coatings on metallic fiber braids. *Journal of Materials Processing Technology*, 192, 97–100.
- Mane, P., Hervig, R., Wadhwa, M., Garvie, L.A.J., Balta, J.B. and McSween, H.Y. (2016) Hydrogen isotopic composition of the Martian mantle inferred from the newest Martian meteorite fall, Tissint. *Meteoritics & Planetary Science*, 51, 2073–2091.
- Mason, H.E., McCubbin, F.M., Smirnov, A. and Phillips, B.L. (2009) Solid-state NMR and IR spectroscopic investigation of the role of structural water and F in carbonate-rich fluorapatite. *American Mineralogist*, 94, 507–516.

- McCubbin, F.M., Boyce, J.W., Srinivasan, P., Santos, A.R., Elardo, S.M., Filiberto, J., Steele, A. and Shearer, C.K. (2016) Heterogeneous distribution of H₂O in the martian interior: Implications for the abundance of H₂O in depleted and enriched mantle sources. *Meteoritics & Planetary Science*, 51, 2036–2060.
- McCubbin, F.M., Hauri, E.H., Elardo, S.M., Vander Kaaden, K.E., Wang, J.H. and Shearer, C.K. (2012) Hydrous melting of the martian mantle produced both depleted and enriched shergottites. *Geology*, 40, 683–686.
- McCubbin, F.M. and Jones, R.H. (2015) Extraterrestrial apatite: Planetary geochemistry to astrobiology. *Elements*, 11, 183–188.
- McCubbin, F.M., Kaaden, K.E.V., Tartèse, R., Klima, R.L., Liu, Y., Mortimer, J., Barnes, J.J., Shearer, C.K., Treiman, A.H., Lawrence, D.J., Elardo, S.M., Hurley, D.M., Boyce, J.W. and Anand, M. (2015a) Magmatic volatiles (H, C, N, F, S, Cl) in the lunar mantle, crust, and regolith: Abundances, distributions, processes, and reservoirs. *American Mineralogist*, 100, 1668–1707.
- McCubbin, F.M., Mason, H.E., Park, H., Phillips, B.L., Parise, J.B., Nekvasil, H. and Lindsley, D.H. (2008) Synthesis and characterization of low-OH- fluor-chlorapatite: A single crystal XRD and NMR spectroscopic study. *American Mineralogist*, 93, 210–216.
- McCubbin, F.M., Shearer, C.K., Burger, P.V., Hauri, E.H., Wang, J.H., Elardo, S.M. and Papike, J.J. (2014) Volatile abundances of coexisting merrillite and apatite in the martian meteorite Shergotty: Implications for merrillite in hydrous magmas. *American Mineralogist*, 99, 1347–1354.
- McCubbin, F.M., Steele, A., Hauri, E.H., Nekvasil, H., Yamashita, S. and Hemley, R.J. (2010) Nominally hydrous magmatism on the Moon. *Proceedings of the National Academy of Sciences of the United States of America*, 27, 11223–11228.
- McCubbin, F.M., Vander Kaaden, K.E., Tartèse, R., Boyce, J.W., Mikhail, S., Whitson, E.S., Bell, A.S., Anand, M., Franchi, I.A., Wang, J.H. and Hauri, E.H. (2015b) Experimental investigation of F, Cl, and OH partitioning between apatite and Fe-rich basaltic melt at 1.0–1.2 GPa and 950–1000 °C. *American Mineralogist*, 100, 1790–1802.
- Mills, S., Mumme, G., Grey, I. and Bordet, P. (2006) The crystal structure of perhamite. *Mineralogical Magazine*, 70, 201–209.
- Mills, S.J., Sejkora, J., Kampf, A.R., Grey, I.E., Bastow, T.J., Ball, N.A., Adams, P.M., Raudsepp, M. and Cooper, M.A. (2011) Krásnoite, IMA 2011-040. *CNMNC Newsletter No. 10*, October 2011. *Mineralogical Magazine*, 75, 2549–2561.
- Mills, S.J., Sejkora, J., Kampf, A.R., Grey, I.E., Bastow, T.J., Ball, N.A., Adams, P.M., Raudsepp, M. and Cooper, M.A. (2012) Krásnoite, the fluorophosphate analogue of perhamite, from the Huber open pit, Czech Republic and the Silver Coin mine, Nevada, USA. *Mineralogical Magazine*, 76, 625–634.
- Oldfield, E., Kinsey, R.A., Smith, K.A., Nichols, J.A. and Kirkpatrick, R.J. (1983) High resolution NMR of inorganic solids: Influence of magnetic centers on magic-angle sample spinning lineshapes in some natural aluminosilicates. *Journal of Magnetic Resonance*, 51, 325–329.
- Pietak, A.M., Reid, J.W., Stott, M.J. and Sayer, M. (2007) Silicon substitution in the calcium phosphate bioceramics. *Biomaterials*, 28, 4023–4032.
- Potts, P.J. and Tindle, A.G. (1989) Analytical characteristics of a multilayer dispersion element (2D = 60Å) in the determination of fluorine in minerals by electron microprobe. *Mineralogical Magazine*, 53, 357–362.

- Prowatke, S. and Klemme, S. (2006) Trace element partitioning between apatite and silicate melts. *Geochimica et Cosmochimica Acta*, 70, 4513–4527.
- Rakovan, J.F. and Pasteris, J.D. (2015) A technological gem: Materials, medical, and environmental mineralogy of apatite. *Elements*, 11, 195–200.
- Raudsepp, M. (1995) Recent advances in the electron microprobe microanalysis of minerals for the light elements. *Canadian Mineralogist*, 33, 203–218.
- Reed, S.J.B. (2005) *Electron Microprobe Analysis and Scanning Electron Microscopy in Geology*. Cambridge University Press, Cambridge, 192 pp.
- Robinson, K.L., Barnes, J.J., Nagashima, K., Thomen, A., Franchi, I.A., Huss, G.R., Anand, M. and Taylor, G.J. (2016) Water in evolved lunar rocks: Evidence for multiple reservoirs. *Geochimica et Cosmochimica Acta*, 188, 244–260.
- Robinson, K.L. and Taylor, G.J. (2014) Heterogeneous distribution of water in the Moon. *Nature Geoscience*, 7, 401–408.
- Rothwell, W.P., Waugh, J.S. and Yesinowski, J.P. (1980) High-resolution variable-temperature ^{31}P NMR of solid calcium phosphates. *Journal of the American Chemical Society*, 102, 2637–2643.
- Sarafian, A.R., Nielsen, S.G., Marschall, H.R., McCubbin, F.M. and Monteleone, B.D. (2014) Early accretion of water in the inner solar system from a carbonaceous chondrite-like source. *Science*, 346, 623–626.
- Sarafian, A.R., Roden, M.F. and Patiño-Douce, A.E. (2013) The volatile content of Vesta: Clues from apatite in eucrites. *Meteoritics & Planetary Science*, 48, 2135–2154.
- Sharp, Z.D., Atudorei, V. and Durakiewicz, T. (2001) A rapid method for determination of hydrogen and oxygen isotope ratios from water and hydrous minerals. *Chemical Geology*, 178, 197–210.
- Sharp, Z.D., Helffrich, G.R., Bohlen, S.R. and Essene, E.J. (1989) The stability of sodalite in the system $\text{NaAlSi}_3\text{O}_8\text{-NaCl}$. *Geochimica et Cosmochimica Acta*, 53, 1943–1954.
- Shearer, C.K., Burger, P.V., Papike, J.J., McCubbin, F.M. and Bell, A.S. (2015) Crystal chemistry of merrillite from Martian meteorites: Mineralogical recorders of magmatic processes and planetary differentiation. *Meteoritics & Planetary Science*, 50, 649–673.
- Shearer, C.K., Papike, J.J., Burger, P.V., Sutton, S.R., McCubbin, F.M. and Newville, M. (2011) Direct determination of europium valence state by XANES in extraterrestrial merrillite. Implications for REE crystal chemistry and martian magmatism. *American Mineralogist*, 96, 1418–1421.
- Siebert, H. (1966) *Anwendungen der Schwingungsspektroskopie in der Anorganischen Chemie*. Anorganische und Allgemeine Chemie in Einzeldarstellungen. Springer Berlin Heidelberg, Berlin, Germany, 209 pp.
- Socrates, G. (2001) *Infrared and Raman characteristic group frequencies: Tables and charts*. John Wiley & Sons, New York, 347 pp.
- Stebbins, J.F. and Zeng, Q. (2000) Cation ordering at fluoride sites in silicate glasses: a high-resolution ^{19}F NMR study. *Journal of Non-Crystalline Solids*, 262, 1–5.
- Sten, Y.E. (1964) Alkali metal monofluorophosphate and calcium carbonate dentifrice. Google Patents.
- Stoeger, B., Weil, M. and Skibsted, J. (2013) The crystal structure of BaPO_3F revisited - a combined X-ray diffraction and solid-state ^{19}F , ^{31}P MAS NMR study. *Dalton Transactions*, 42, 11672–11682.

- Tait, K.T., Barkley, M.C., Thompson, R.M., Origlieri, M.J., Evans, S.H., Prewitt, C.T. and Yang, H.X. (2011) Bobdownsite, a new mineral species from Big Fish River, Yukon, Canada, and its structural relationship with whitlockite-type compounds. *Canadian Mineralogist*, 49, 1065–1078.
- Tartèse, R., Anand, M., Barnes, J.J., Starkey, N.A., Franchi, I.A. and Sano, Y. (2013) The abundance, distribution, and isotopic composition of Hydrogen in the Moon as revealed by basaltic lunar samples: implications for the volatile inventory of the Moon. *Geochimica et Cosmochimica Acta*, 122, 58–74.
- Tartèse, R., Anand, M., Joy, K.H. and Franchi, I.A. (2014a) H and Cl isotope systematics of apatite in brecciated lunar meteorites Northwest Africa 4472, Northwest Africa 773, Sayh al Uhaymir 169, and Kalahari 009. *Meteoritics & Planetary Science*, 49, 2266–2289.
- Tartèse, R., Anand, M., McCubbin, F.M., Elardo, S.M., Shearer, C.K. and Franchi, I.A. (2014b) Apatites in lunar KREEP basalts: The missing link to understanding the H isotope systematics of the Moon. *Geology*, 42, 363–366.
- Taylor, C.M., Taylor multi element standard documentation. C.M. Taylor Company (no longer in business).
- Terpstra, P. (1937) On the crystallography of brushite. *Zeitschrift Fur Kristallographie*, 97, 229–233.
- Tondu, J.M.E., Turner, K.W., Wolfe, B.B., Hall, R.I., Edwards, T.W.D. and McDonald, I. (2013) Using Water Isotope Tracers to Develop the Hydrological Component of a Long-Term Aquatic Ecosystem Monitoring Program for a Northern Lake-Rich Landscape. *Arctic Antarctic and Alpine Research*, 45, 594–614.
- Treiman, A.H., Boyce, J.W., Gross, J., Guan, Y.B., Eiler, J.M. and Stolper, E.M. (2014) Phosphate-halogen metasomatism of lunar granulite 79215: Impact-induced fractionation of volatiles and incompatible elements. *American Mineralogist*, 99, 1860–1870.
- Turner, G.L., Smith, K.A., Kirkpatrick, R.J. and Oldfield, E. (1986) Structure and cation effects on phosphorus-31 NMR chemical shifts and chemical-shift anisotropies of orthophosphates. *Journal of Magnetic Resonance*, 70, 408–415.
- Wang, F. and Grey, C.P. (1998) Probing the defect structure of anion-excess $\text{Ca}_{1-x}\text{Y}_x\text{F}_{2+x}$ ($x = 0.03\text{--}0.32$) with high-resolution ^{19}F magic-angle spinning nuclear magnetic resonance spectroscopy. *Chemistry of Materials*, 10, 3081–3091.
- Webster, J.D. and Piccoli, P.M. (2015) Magmatic apatite: A powerful, yet deceptive, mineral. *Elements*, 11, 177–182.
- Weil, M., Baran, E.J., Kremer, R.K. and Libowitzky, E. (2015) Synthesis, crystal structure, and properties of $\text{Mn}(\text{PO}_3\text{F})\cdot 2\text{H}_2\text{O}$. *Zeitschrift Fur Anorganische Und Allgemeine Chemie*, 641, 184–191.
- Weil, M., Puchberger, M. and Baran, E.J. (2004) Preparation and characterization of dimercury(I) monofluorophosphate(V), $\text{Hg}_2\text{PO}_3\text{F}$: Crystal structure, thermal behavior, vibrational spectra, and solid-state ^{31}P and ^{19}F NMR spectra. *Inorganic Chemistry*, 43, 8330–8335.
- Weil, M., Puchberger, M., Fueglein, E., Baran, E.J., Vannahme, J., Jakobsen, H.J. and Skibsted, J. (2007) Single-crystal growth and characterization of disilver(I) monofluorophosphate(V), $\text{Ag}_2\text{PO}_3\text{F}$: Crystal structure, thermal behavior, vibrational spectroscopy, and solid-state ^{19}F , ^{31}P , and ^{109}Ag MAS NMR spectroscopy. *Inorganic Chemistry*, 46, 801–808.
- Yapp, C.J. (1985) D/H variations of meteoric waters in Albuquerque, New Mexico, USA. *Journal of Hydrology*, 76, 63–84.

- Yesinowski, J.P. and Eckert, H. (1987) Hydrogen environments in calcium phosphates ^1H MAS NMR at high spinning speeds. *Journal of the American Chemical Society*, 109, 6274–6282.
- Zeibig, M., Wallis, B., Mowius, F. and Meisel, M. (1991) Salts of 17 halogenophosphoric acids: Preparation and crystal structure of copper(II) monofluorophosphate dihydrate $\text{CuPO}_3\text{F}\cdot 2\text{H}_2\text{O}$. *Zeitschrift Fur Anorganische Und Allgemeine Chemie*, 600, 231–238.
- Zhang, L., de Araujo, C.C. and Eckert, H. (2007) Structural role of fluoride in aluminophosphate sol-gel glasses: High-resolution double-resonance NMR studies. *Journal of Physical Chemistry B*, 111, 10402–10412.
- Zhang, W.P., Sun, M.Y. and Prins, R. (2002) Multinuclear MAS NMR identification of fluorine species on the surface of fluorinated γ -alumina. *Journal of Physical Chemistry B*, 106, 11805–11809.

Tables

Table 1. Average electron microprobe analyses of phosphates analyzed in present study

Oxide	Yukon					
	Bobdownsite_A	phosphate	Bobdownsite_Tait	R050109	R070654	MGS-008
P ₂ O ₅	45.52 (71)	46.6 (2)	46.94 (39)	47.07 (29)	46.03 (52)	46.98 (66)
SiO ₂	0.09 (3)	0.00 (0)	0.10 (10)	0.00 (0)	0.00 (0)	0.00 (0)
Al ₂ O ₃	0.37 (12)	0.34 (14)	0.30 (15)	0.01 (1)	0.00 (0)	n.d.
FeO	1.09 (11)	1.10 (19)	1.43 (40)	1.33 (10)	0.01 (1)	0.00 (0)
MnO	0.02 (1)	0.01 (1)	0.02 (2)	0.02 (1)	0.02 (3)	0.00 (0)
MgO	2.87 (8)	2.88 (13)	2.63 (19)	2.77 (11)	3.53 (8)	3.75 (10)
CaO	47.19 (50)	46.5 (2)	47.04 (40)	47.46 (21)	47.88 (19)	47.65 (36)
Na ₂ O	0.51 (22)	1.00 (31)	0.72 (29)	0.61 (18)	0.19 (0.04)	0.00 (0)
H ₂ O	0.71 (4)	0.70 (5)	<i>n.d.</i>	<i>n.d.</i>	<i>n.d.</i>	<i>n.d.</i>
SO ₃	0.00 (0)	<i>n.d.</i>	<i>n.d.</i>	<i>n.d.</i>	<i>n.d.</i>	0.16 (9)
F	0.00 (0)	0.00 (0)	0.00 (0)	0.00 (0)	0.00 (0)	n.d.
Cl	0.00 (0)	0.00 (0)	0.01 (1)	0.00 (0)	0.00 (0)	0.01 (1)
-O ≡ F	0	0	0	0	0	-
-O ≡ Cl	0	0	0	0	0	0
Total	98.37	99.2	99.20	99.26	97.65	99.41
N	78	54	66	101	102	10
<i>Structural formulae based on 28 oxygens</i>						
P	6.92	7.01	7.01	7.03	6.97	6.99
Si	0.02	0.00	0.02	0.00	0.00	0.00
Al	0.08	0.07	0.06	0.00	0.00	-
Fe	0.16	0.16	0.21	0.20	0.00	0.00
Mn	0.00	0.00	0.00	0.00	0.00	0.00
Mg	0.77	0.76	0.69	0.73	0.94	0.98
Ca	9.09	8.86	8.90	8.98	9.18	8.98
Na	0.18	0.34	0.25	0.21	0.07	0.00
S	0.00	-	-	-	-	0.02
∑ Cations	17.22	17.21	17.14	17.14	17.16	16.95
F	0.00	0.00	0.00	0.00	0.00	-
Cl	0.00	0.00	0.00	0.00	0.00	0.00
∑ Anions						
OH	0.86	0.83	0.85*	0.85*	0.85*	1.00 [‡]

N – number of analyses

- signifies that a value was not computed

n.d. – abundance was not determined

*Value is based on the average OH from Bobdownsite_A and Yukon phosphate to aid in accurate structural formula determination

[‡]Value is assumed based on stoichiometry and used to calculate an appropriate structural formula

Parenthetical values represent the uncertainty in the reported abundance

Figures

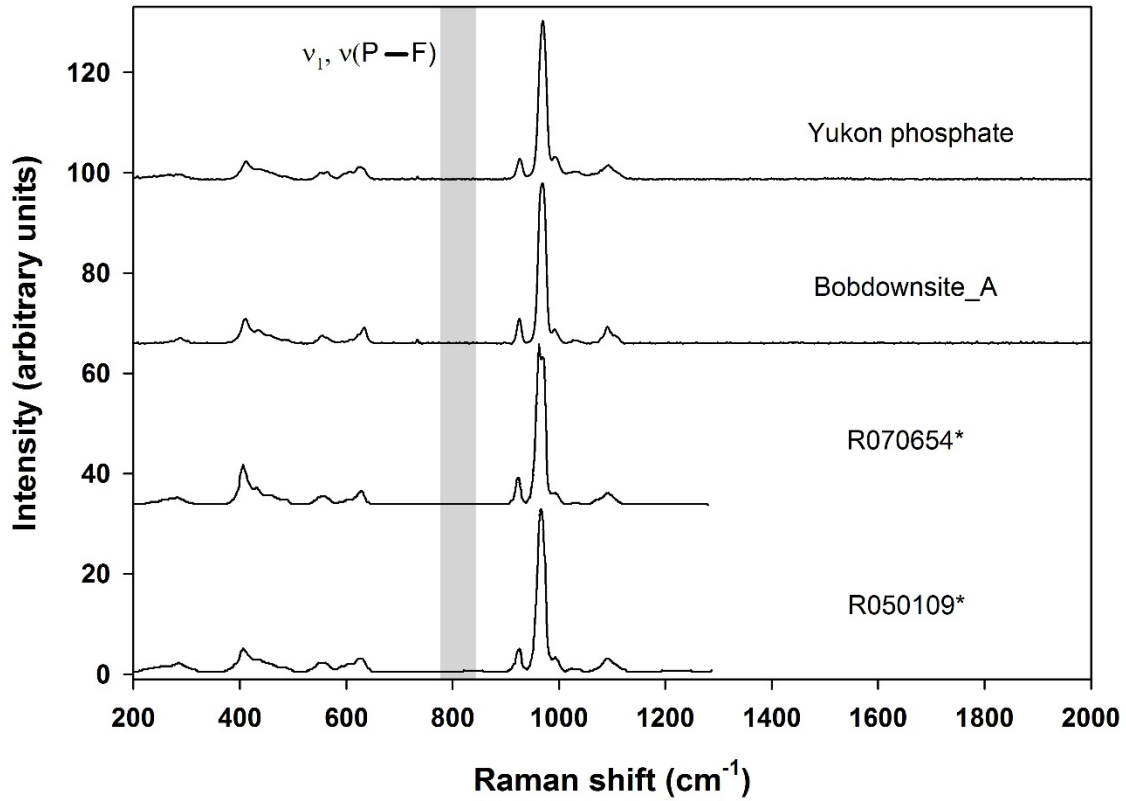


Figure 1. Raman spectra of Yukon phosphate, Bobdownsite_A, bobdownsite type specimen R050109, and bobdownsite from Tip top Mine, South Dakota, USA (R070654). The sample names denoted with an asterisk indicate the data were reported in Tait et al. (2011). The region that is characteristic of P-F symmetric stretching modes in fluorophosphate salts is indicated by the shaded area (Baran and Weil, 2009; Heide et al., 1985; Jantz et al., 2016; Weil et al., 2015; Weil et al., 2004; Weil et al., 2007; Zeibig et al., 1991).

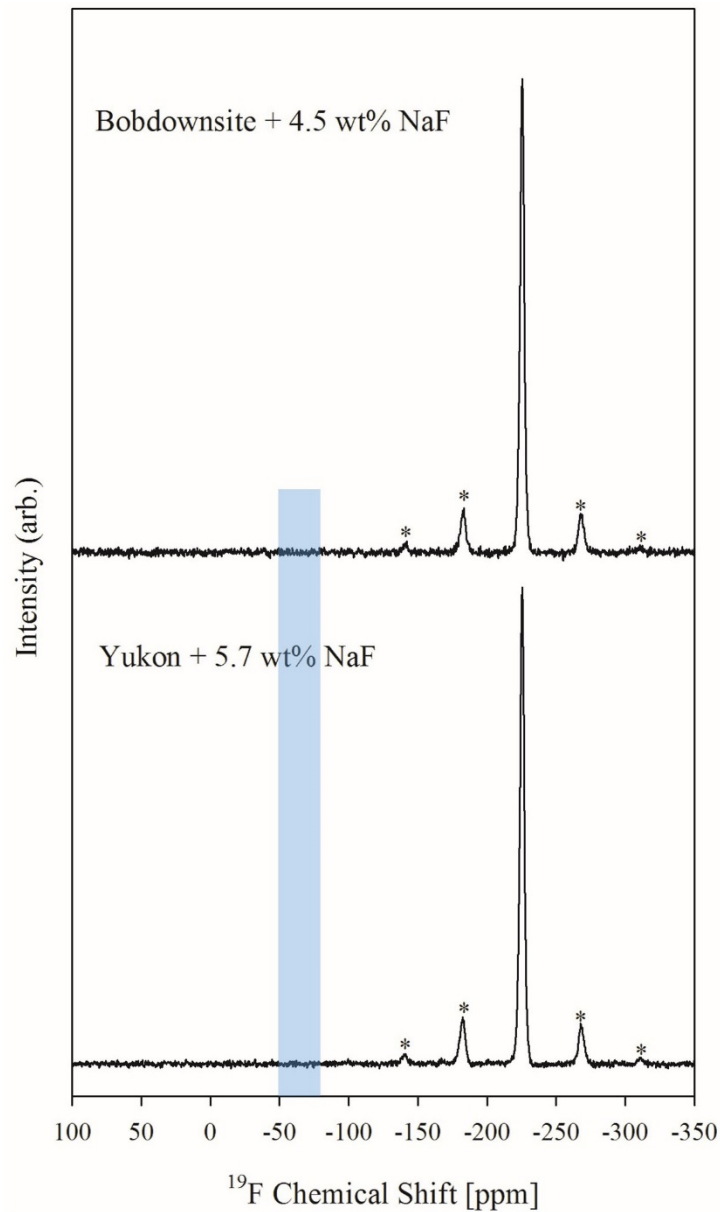


Figure 2. ^{19}F MAS/NMR spectra of Bobdownsite_A (top) and Yukon phosphate (bottom) samples with the indicated amounts of added NaF, which approximate one F atom per formula unit (seven P). Shaded region corresponds to chemical shift range for previous reports of compounds containing fluorophosphate groups (see text). Spectra acquired by direct excitation with a 100 s relaxation delay and a spinning rate of 20 kHz. Asterisks denote spinning sidebands.

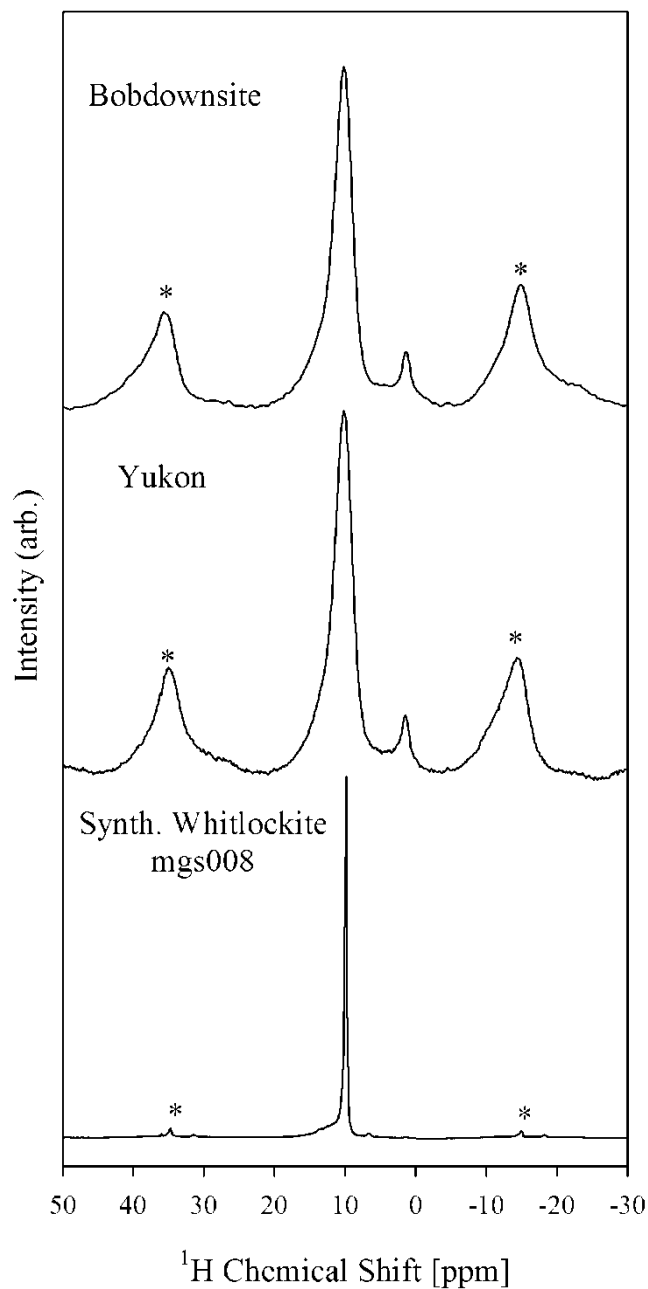


Figure 3. Comparison of the center band region of ^1H MAS/NMR spectra of Bobdownsite_A (top) and Yukon phosphate (middle) specimens and synthetic whitlockite sample MGS-008 (bottom). Spectra acquired by direct excitation with a 30 s relaxation delay at a spinning rate of 10 kHz. Spinning sidebands are denoted by asterisks and for the natural phosphate samples extend for at least four more orders owing to broadening by paramagnetic ions.

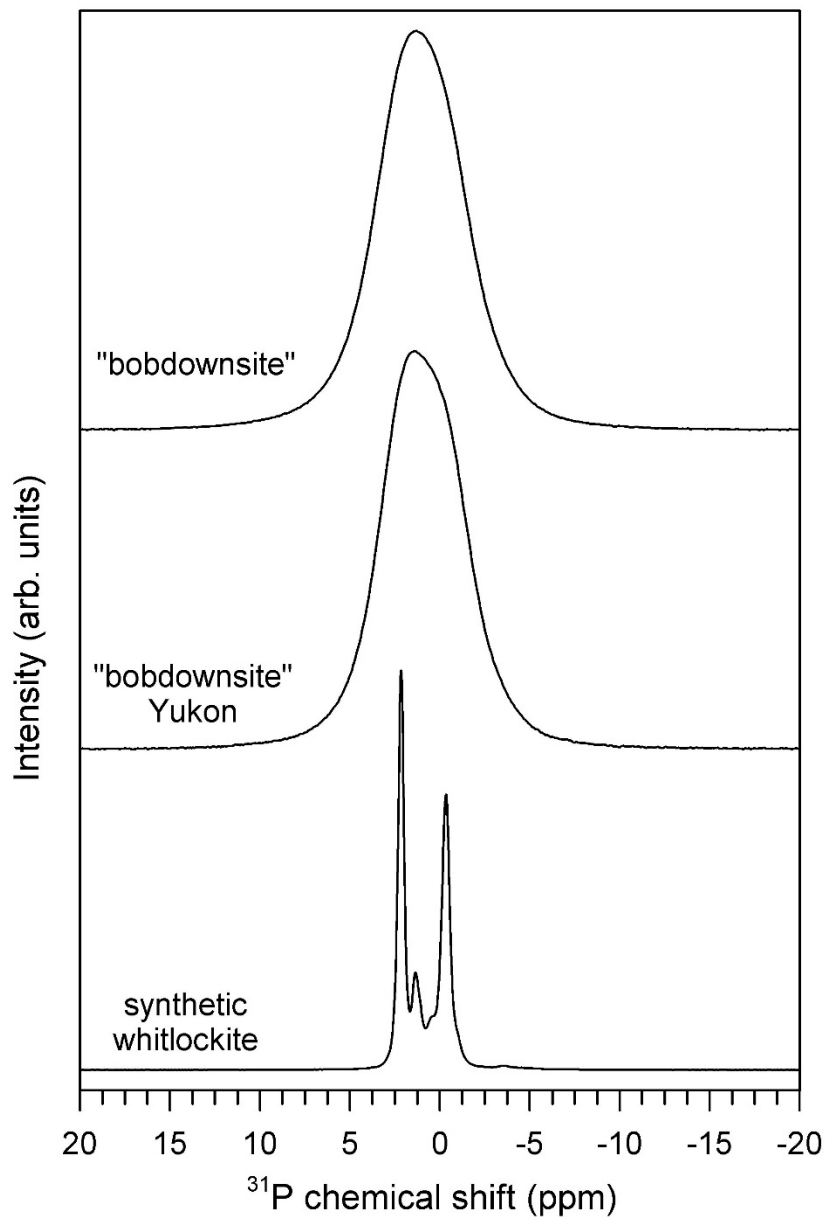


Figure 4. Comparison of ^{31}P SP-MAS NMR spectra of Bobdownsite_A (top) and Yukon phosphate (middle) specimens and synthetic whitlockite sample MGS-008 (bottom). Spectra were acquired with direct excitation (single-pulse) with a 300 s relaxation delay at a spinning rate of 15 kHz. Spinning sidebands fall outside the displayed spectral region. Highly resolved spectra for synthetic samples result from absence of paramagnetic substituents.